

Hyperviscous diblock copolymer vesicles

R. Dimova^{1,2,a}, U. Seifert^{1,4}, B. Pouligny², S. Förster³, and H.-G. Döbereiner¹

¹ Max-Planck-Institut für Kolloid- und Grenzflächenforschung, Am Mühlenberg 1, 14476 Golm, Germany

² Centre de Recherche Paul Pascal, CNRS, Pessac 33600, France

³ Universität Hamburg, Institut für Physikalische Chemie, Bundesstraße 45, 20145 Hamburg, Germany

⁴ Universität Stuttgart, Institut für Theoretische Physik II, Pfaffenwaldring 57, 70550 Stuttgart, Germany

Received 2 March 2001 and Received in final form 15 February 2002

Abstract. Giant vesicles prepared from the diblock copolymer polybutadien-b-polyethyleneoxide (PB-PEO) exhibit a shear surface viscosity, which is about 500 times higher than those found in common phospholipid bilayers. Our result constitutes the first direct measurement of the shear surface viscosity of such polymersomes. At the same time, we measure bending and stretching elastic constants, which fall in the range of values typical for lipid membranes. Pulling out a tether from an immobilized polymersome and following its relaxation back to the vesicle body provides an estimate of the viscous coupling between the two monolayers composing the polymer membrane. The detected intermonolayer friction is about an order of magnitude higher than the characteristic one for phospholipid membranes. Polymersomes are tough vesicles with a high lysis tension. This, together with their robust rheological properties, makes them interesting candidates for a number of technological applications.

PACS. 83.50.Lh Slip boundary effects (interfacial and free surface flows) – 83.85.Jn Viscosity measurements – 87.16.Dg Membranes, bilayers, and vesicles – 87.80.Cc Optical trapping

1 Introduction

Bilayer membranes are probably the best-studied supramolecular architecture employed in nature. Indeed, in their biological relevant state most lipids form fluid membranes, which provide the boundaries of cellular organelles and for the cell itself. However, under appropriate conditions many other amphiphilic molecules self-assemble in an aqueous environment into bimolecular sheets. These bilayer membranes may close up into vesicles or form bulk lamellar phases. A particular interesting class of molecules are linear amphiphilic diblock copolymers. Whereas their thermodynamic phases as melts are reasonably well understood [1], their lyotropic behavior is only beginning to emerge [2,3]. Recently, single giant vesicles could be swollen from polyethylethylene-polyethyleneoxide (PEE-PEO) in aqueous solution [4]. These, so-called polymersomes, were used to characterize the elastic properties of polymer membranes. However, not much is known about other properties. Their viscous behavior, which will be the focus of this paper, has not been studied before.

In contrast, physical properties of lipid bilayers are well documented [5,6]. In particular, there is a long history of research papers elucidating membrane elasticity

and morphology as well as membrane viscosity [7]. Elastic deformations of a membrane include bending, stretching and shear. For lipids in fluid phase, bending elastic moduli are found to be on the order of $10 k_B T$. Thus, lipid membranes are subject to thermally excited fluctuations of their morphological conformation. Stretching a membrane is considerably harder in comparison. There is a constant equilibrium membrane area at zero external force. Typically, stretching elastic moduli are measured to be on the order of 100 dyn/cm. Polymer membranes have similar elastic properties, except that they are much tougher than lipids, *i.e.*, they are considerably harder to break under tension [4]. Response to shear depends on the state of the membrane. Lipids are known to undergo a gel-fluid transition with temperature. In the gel state, lipid membranes possess finite shear elasticity. Above the transition temperature, in the fluid state, there is no static resistance to shear. However, membranes do oppose shear deformations dynamically. Typically, one finds surface viscosities on the order of 10^{-6} dyn s/cm [8,9]. In contrast, our polymer membranes are much more viscous with a three orders of magnitude larger surface viscosity. Nevertheless, the membranes studied are in a fluid state, well above the glass transition.

Thus, diblock-copolymer membranes show toughness against mechanical stress and robust rheological behavior. These properties as well as the absence of a ther-

^a e-mail: dimova@mpikg-golm.mpg.de

mal transition of their membrane at ambient temperatures and in the physiological temperature range make them an exciting new class of materials. Indeed, diblock-copolymer vesicles were shown to be quite promising for biomedical applications like drug delivery [10]. Essential for encapsulation and delivery of agents are the thermo-mechanical characteristics of the transporting unit [11]. The properties of the carrier shell have to be within certain limits of stability, stiffness, permeability, etc. Compared to lipids, polymer chemistry allows to design these properties relatively easily. Further, the use of polymersomes is not limited to biomedical applications in aqueous environments; other solvent systems have been explored as well [12].

For our study we employ giant vesicles made from the diblock polybutadiene-*b*-polyethyleneoxyde (PB-PEO, $s\text{-Bu-}[\text{CH}_2\text{-CH}(\text{C}_2\text{H}_5)]_{32}\text{-}[\text{O-CH}_2\text{-CH}_2]_{20}\text{-OH}$) [13]. Compared to ethylene, butadiene has an additional double bond allowing polymerization of the membrane via ultraviolet radiation. Giant vesicles were chosen as an ideal system for studying fundamental properties of bilayer membranes [14]. Due to their relatively large size, they are readily visible under a microscope and allow direct observation.

To set the stage for our experimental results and later data analysis, we discuss now the physics of viscous dissipation in a vesicle system. The general response of a vesicle membrane to the application of an external force or a thermal kick involves flow of water due to the displacement of the membrane surface, flow of molecules inside the bilayer membrane and relative movement of the two monolayers with respect to each other. There is viscous energy loss in all three cases characterized by bulk water viscosity, membrane surface viscosity and interlayer drag [15–17], and in the latter two dissipation occurs within the membrane. For phospholipid vesicles dissipation in the bulk water is dominant on length scales accessible with video microscopy. Only modes below a micron are subject to membrane dissipation. In contrast, for polymer membranes the effects of both membrane dissipative mechanisms are significantly larger. Hence, one expects that even shape fluctuations above the micron scale are strongly affected if not dominated by membrane dissipation.

We measured surface viscosity by observing the movement of a latex particle attached to a vesicle membrane [8, 9, 18]. Either the particle was allowed to sediment under gravity along the vesicle surface (falling-ball viscosimetry) or was pulled into an optical trap placed slightly off-center from the bead (optical dynamometry). Further, we employed tether-pulling experiments [15, 19–21] in order to probe intermonolayer drag [19]. Extracting a tether from a giant vesicle is a versatile technique. It not only gives information on viscous properties [22] and flip-flop rates [21, 23] but also allows to characterize membrane bending elasticity [15, 24, 25]. Elastic moduli as well as membrane spontaneous curvature [26, 27] can be measured on a nanometer length scale. Earlier, monolayer coupling had been monitored via fluorescence recovery after photobleaching in supported bilayers [28]. We employed micropipette aspiration [29–31] to obtain elastic bending and stretching

moduli. They are deduced from the observation of vesicle membrane extension into pipettes with diameters of several micrometers as a function of suction pressure.

After detailing polymer preparation and experimental techniques used, we present our results on viscoelastic behavior of polymer membranes. Extended new theoretical analysis is performed on tether-pulling data of highly viscous membranes. The paper closes with a discussion and an outlook.

2 Experimental procedures

The diblock copolymer used here was synthesized according to Förster and Krämer (1999) [13]. The molecular-weight distribution was determined by Gel Permeation Chromatography. The weight polydispersity was $M_w/M_n \approx 1.05$, where M_n and M_w are, respectively, the number and the weight average molecular weights. The ratio of 1,2- *versus* 1,4-butadiene is 9:1. The dry polymer melt was stored in the freezer at -20°C . Stock solutions were made using chloroform.

2.1 Vesicle preparation

Vesicles were prepared either by electroformation [32] or by a standard swelling procedure [30]. For the electroformed vesicles we used a glass chamber with two platinum electrodes connected to an electric-field generator. A few microliters of the polymer solution (1 mg/ml dissolved in chloroform) were initially deposited on both electrodes and dried under vacuum over night. Then, after applying an AC field of 5 V and 10 Hz for a period of 10 minutes, water was introduced in the chamber and the amplitude was gradually increased up to 9 V within the next 10 minutes. Preparation time did not exceed 30 minutes. The average radius of the formed vesicles was about 40 μm . Applying lower voltages, ca. 800 mV, for the electroformation yielded smaller vesicles with no difference in the rheological characteristics. Higher voltages were preferably used because the growing times were thereby significantly reduced—from about 3 hours at 800 mV to 15 minutes at 9 V.

In the swelling procedure a few drops (about 30 μl) of the polymer solution (40 mg/ml in chloroform) were spread on a roughened Teflon plate and dried under vacuum. The sample was prehydrated and swollen in 100 mM sucrose solution. The total preparation time was about 3 days. The formed vesicles were generally of smaller radius (about 15 μm on the average) but exhibited more excess area than the electroformed vesicles, which were mainly spherical.

Preparation of vesicles following the two different protocols was necessitated from the requirements imposed by the micropipette aspiration and the viscosity measurements. Vesicles for pipette aspiration need to have enough excess surface area to allow extension of the membrane into the pipette. Therefore, these vesicles were prepared

by swelling on Teflon. For the viscosity measurement, vesicles need to have very little excess surface area (see below), which is achieved with the electroformation method. The vesicles for micropipette aspiration were observed with an inverse microscope (Axiovert 135 from Carl Zeiss). As an illumination source in both, micropipette and viscosity, measurements we used a halogen lamp with a wide-band green filter.

Temperature scans on polymer solutions performed with a differential scanning calorimeter (Microcal) did not show any signs of a phase transition of the polymer in the 5° to 60°C temperature interval. Of course, this does not rule out possible slight changes of the material properties.

2.2 Elasticity measurements

Elastic properties of PB-PEO membranes were studied via micropipette aspiration of slightly deflated vesicles prepared by the standard swelling procedure [30]. The experimental chamber was pre-coated with albumin (1 mg/ml) to avoid adhesion of the vesicles to the glass walls, and then filled with a glucose solution¹. Several tens of microliters of the vesicle suspension were transferred into the experimental chamber. Temperature was regulated by means of a circulating-water jacket connected to a thermostat. The micropipette experiments were performed at 10°C to minimize evaporation from the experimental chamber. We used an open chamber to allow access for micropipettes. Shortly, the experimental procedure consists in aspirating a vesicle, applying different suction pressures and measuring the area response of the vesicle membrane. Aspiration was realized by means of a hydrostatic pressure system with a motorized computer-controlled vertical stage [31]. The suction pressures ranged from 10 to 2×10^4 dyn/cm². Micropipettes were generally produced with a radius of about 4 μm. Manipulating vesicles with thinner pipettes proved to be inefficient —tension could cause instability and pinching of the surface aspirated in the pipette. With larger pipettes the accuracy of measuring the area change was lower. In order to determine the variation in the vesicle area, we followed the evolution of three geometrical parameters: the radius of the outer vesicle portion, the projection length inside the pipette and the position of the tip of the pipette. The latter was used to monitor the pipette location in order to correct for possible shifts during measurements. We calibrated our setup by measuring elastic moduli for the standard lipid stearyllecylphosphatidylcholine. Consistent with literature values, we obtained $k_C = 30 \pm 4k_B T$ for the bending modulus [33,34] and $K_a = 230 \pm 10$ dyn/cm for the stretching modulus [34] in sucrose/glucose solution.

¹ The difference between the refractive indices of glucose and sucrose (swelling solvent) allows for better observation of the vesicles.

2.3 Viscosity measurements

Two different experimental approaches were applied for measuring shear surface viscosity of the polymer membrane: falling-ball viscosimetry [8,9,18] and optical dynamometry [9]. Both of these techniques make use of a latex particle (Polyscience, Warrington, PA). The latex sphere is attached to the membrane. (We chose to work with vesicles of size generally larger than 50 μm in radius.) The bead intercepts the vesicle surface in a disc the radius of which depends on the particle penetration towards the vesicle interior; see Figure 1. The particle motion along the membrane is tracked. The vesicles used for the viscosity measurements were prepared by electroformation. The study was performed at room temperature.

The particle radius was measured prior to adhesion to the vesicle. The bead was let to sediment freely in bulk water. We measured the falling velocity v_{free} . Stokes law provides the particle radius: $R_b = \sqrt{\frac{9\eta v_{\text{free}}}{2\Delta\rho g}}$, where η is the water viscosity at the corresponding temperature, $\Delta\rho$ is the latex-water density difference ($\cong 0.05$ g/ml; it was measured via centrifugation of particles in glycerol solutions), and g is the gravitational acceleration.

The experimental procedure starts with bringing the latex bead (of radius about 5 μm) to a previously selected vesicle by means of a long-distance-working optical trap. (The setup design is described in [35].) The latter consists of two counter-propagating laser beams focused inside the experimental chamber. When brought into the vicinity of the membrane, the particle spontaneously sticks to it and can no longer be detached by the optical-trap forces (a few tens of piconewtons). The dynamics of the adhesion process was studied in detail by Dietrich *et al.* [36]. Finally, the bead attains a fixed position normal to the membrane and can be displaced only tangentially along the vesicle surface.

In the falling-ball viscosimetry method [8,9,18], after attaching the particle to the membrane, we bring it to the upper hemisphere of the vesicle by means of the trap (Fig. 1a). Then, the bead is released and its sedimentation path towards the vesicle bottom is recorded. We observe the system from above. The image is refocused to follow the falling particle. The sedimentation velocity contains the desired information about the membrane viscosity [8,18].

The second technique used for the extraction of the membrane viscosity, optical dynamometry, is based on following the particle movement under the action of the radiation pressure force of the optical trap. First, the particle is brought to a pole of the vesicle, where the bead basically “sees” the membrane as horizontal and flat. Then the optical trap is switched off and displaced about one particle radius. After switching the laser beams on again, the radiation pressure creates an attraction field that drags the particle toward the laser beams axis (Fig. 1c). The trajectory of the particle is recorded. The measured parameter is the drag coefficient of the particle motion. The radiation pressure was calibrated for each of the employed particles prior to adhesion in the following manner: The bead was

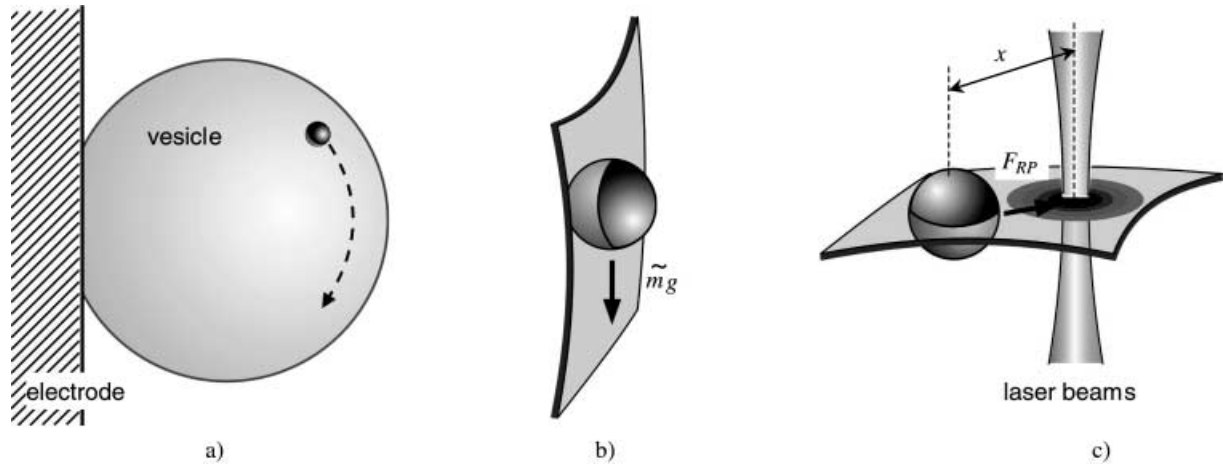


Fig. 1. a) Falling-ball viscosimetry. A particle attached to the vesicle membrane sediments towards the vesicle bottom. b) Close-up view of the particle at the vesicle equator; there we measure the maximal sedimentation velocity. c) Optical-trap dynamometry. The sketch is exaggerated in terms of distances —the trap is usually positioned at the particle periphery.

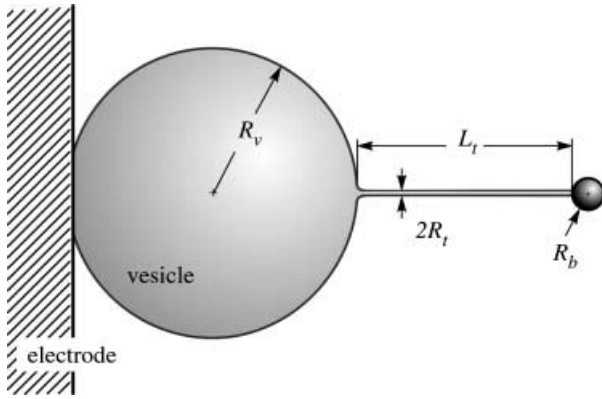


Fig. 2. Tether-pulling experiment. The vesicle is attached to the electrode. The radius of the tether is magnified for clarity.

subjected to a flow of constant velocity. From the lowest speed at which the particle escapes the optical trap one can determine the optical force by balancing it with the Stokes resistance. The radiation pressure force can be also computed by applying the Generalized Lorenz-Mie theory (for details on trapping force determination see [9]). Both approaches give consistent results.

2.4 Tether-pulling experiments

The last experimental scenario deals with tether formation out of a vesicle (Fig. 2). We worked with vesicles, which were tightly attached (thus immobile) to the electrode of the electroformation chamber. Pulling out a tether was done with a latex particle of small penetration depth in the vesicle (small contact area)². By displacing the attached particle with the optical trap we pulled out the tether. The applied forces were on the order of several tens of piconewtons. After releasing the latex bead, it moves back

² When pulling particles with large penetration we could form short tubes of radius of about 5 μm .

towards the vesicle body dragged by the retracting tether. The particle trajectory back to the vesicle was recorded as a function of time.

3 Results and data analysis

3.1 Micropipette aspiration: bending and stretching elasticity

For the micropipette experiments we selected vesicles that were slightly deflated, *i.e.*, exhibiting excess surface area. We trapped a vesicle applying low suction pressure and followed the evolution in the vesicle area by increasing the aspiration pressure, *i.e.*, the surface tension τ . For calculating the membrane area A , we considered the aspirated vesicle as a geometrical body, where the part of the vesicle inside the pipette is described as a cylinder with a hemispherical cap of radius equal to the internal pipette radius.

We were interested in two modes of deformation: at low tensions (entropic regime) the thermal fluctuations of the membrane are gradually flattened out; in the high-tension regime the membrane is stretched. The relative area change in the entropic regime [29,37] is described by

$$\frac{A - A_0}{A_0} = \frac{k_B T}{8\pi k_C} \ln \tau / \tau_i, \quad (1)$$

where A_0 is the initial projected area of the vesicle, $k_B T$ is the thermal energy, k_C is the bending elasticity modulus and τ_i is the initial tension at which $A = A_0$. Figure 3a presents data collected from six vesicles. The slope of the linear fit for low tensions provides the value of k_C . We find it to be $42 \pm 5 k_B T$.

In the high-tension regime, vesicle stretching [29,37] is described by

$$\frac{A - A_0}{A_0} = \frac{\tau}{K_a}, \quad (2)$$

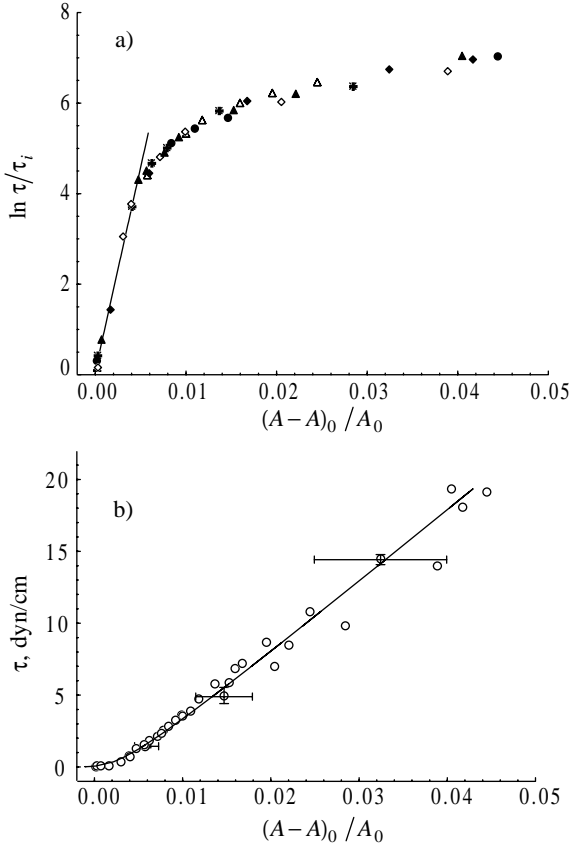


Fig. 3. Elastic properties of polymer vesicles measured via micromanipulation with pipettes. a) Entropic regime (smoothing the vesicle fluctuations): The slope of the solid line according to equation (1) provides k_C ; $\tau_i = 0.02$ dyn/cm; the symbols present data from different vesicles. b) High-tension regime of membrane stretching. The solid curve is a fit over the entire interval of tensions assuming a superposition of bending and stretching elasticities (Eqs. (1) and (2)); $k_C = 42 \pm 5k_B T$ and $K_a = 470 \pm 15$ dyn/cm.

where K_a is the stretching elasticity constant. The same data as in Figure 3a is plotted in linear τ -scale in Figure 3b with the experimental error indicated. The slope of a linear fit in the high-tension region gives $K_a = 450 \pm 85$ dyn/cm. For fitting the entire range of tension one can assume a superposition of the two contributions —elastic bending and stretching [29,34]. The solid curve in Figure 3a is a fit where $k_C = 42 \pm 5k_B T$ and $K_a = 470 \pm 15$ dyn/cm. We estimate the crossover tension between the two regimes $\tau_c \equiv \frac{K_a k_B T}{8\pi k_C} \cong 0.5$ dyn/cm. Even the highest induced tensions (about 23 dyn/cm) were insufficient for rupturing the vesicle membrane. Compared to lipid bilayers where lysis tension is typically lower than 10 dyn/cm [30], polymersomes appear to be more resistant to rupture.

3.2 Falling-ball viscosimetry

After being brought to the upper hemisphere of the vesicle and released from the trap, the latex particle sediments

towards the bottom of the vesicle. The resistance experienced by the bead is characterized by the drag coefficient ζ . The bead trajectory can be described exactly by an analytical solution of the equation of motion; see [18] and [8]. For the purpose of analyzing experiments on polymersomes, it suffices to determine the maximal sedimentation velocity detected at the vesicle equator. There the particle weight exactly balances the friction —see Figure 1b (otherwise the gravitational force enters the force balance through its projection onto the vesicle surface),

$$\tilde{m}g = \zeta v_{\text{eq}} \quad , \quad (3)$$

where \tilde{m} is the particle mass corrected for buoyancy and v_{eq} is the particle sedimentation velocity at the vesicle equator. The drag coefficient ζ contains information about the shear surface viscosity of the membrane η_s . Deducing η_s from ζ requires computing the hydrodynamic flow around the particle when it moves along the spherical surface. The theoretical approach was presented elsewhere [38]. Detailed analysis [8] showed the presence of finite-size effects, *i.e.*, increased friction due to recirculation of the water enclosed in the vesicle. These effects, however, are negligible for the systems discussed here. We worked with vesicles more than 10 times larger than the latex particles and for most of the systems the membrane was intercepting the latex bead through the bead center (*i.e.*, through the bead equator). Therefore, the particles could be considered as moving on a flat surface. In this case, one may estimate η_s from ζ by means of the following empirical relation³:

$$\zeta = 6\pi\eta R_b + 2.93\eta_s \left(\frac{\eta_s}{\eta R_b} \right)^{-0.12} \quad , \quad (4)$$

which is an approximation of the numerical solution of the problem [8,38]. R_b is the bead radius. Doing so, we obtain for the shear surface viscosity of polymer membranes $\eta_s \cong 1.5 \times 10^{-3}$ dyn s/cm. This value is reproduced to within $\pm 8\%$ when the experiment is repeated many times on different vesicles.

3.3 Optical dynamometry

The driving force in optical dynamometry is the radiation pressure force F_{RP} , exerted by the optical trap (Fig. 1c). For distances smaller than about $0.6 R_b$, F_{RP} is approximately proportional to the trap-bead distance x : $F_{\text{RP}} = k_{\text{RP}} x$, where k_{RP} is the radiation pressure spring constant. The force balance for the attracted bead gives

$$0 = k_{\text{RP}} x - \zeta \dot{x} \quad . \quad (5)$$

The solution reads

$$x(t) = x_0 \exp(-t/t_c) \quad , \quad (6)$$

³ Note that the units of the shear surface viscosity are [bulk viscosity] \times [layer thickness].

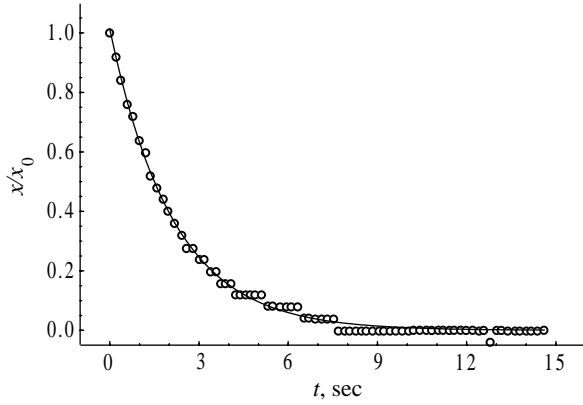


Fig. 4. Optical-trapping dynamics. Scaled distance between the particle and the laser beam axis (see Fig. 1c) *versus* time. The solid curve is a fit according to equation (6) with $t_c = 2.1$ s.

where x_0 is the initial distance between the bead center and the trap axis and $t_c = \zeta/k_{\text{RP}}$ is the characteristic time of the process. We worked with particles whose centers were lying in the plane of the membrane and therefore the applied radiation pressure force was not inducing out-of-plane deformations as discussed in [9]. Figure 4 shows an example of the reduced particle-trap distance (x/x_0) after switching on the optical trap. The particle was of radius $5.24 \mu\text{m}$ and was penetrating the vesicle so that the membrane intercepted the bead through its equator (the contact angle was close to 90°). Because the vesicle was large (about $120 \mu\text{m}$ in radius) we may assume the membrane as flat. The exponential fit provides $t_c = 2.1$ s for the characteristic time of the process. For this measurement $k_{\text{RP}} = 1.21 \times 10^{-3}$ dyn/cm. From the characteristic time we estimate ζ . To deduce the shear surface viscosity from the friction coefficient we apply equation (4). The average value from all optical dynamometry measurements is $\eta_s \cong (1.7 \pm 0.3) \times 10^{-3}$ dyn s/cm, which is in very good agreement with the results from falling-ball viscosimetry measurements.

3.4 Tether pulling: intermonolayer friction

A sketch of the vesicle-tether geometry is presented in Figure 2. We denote the vesicle radius R_v . The tether is assumed to be a cylindrical tube [26] made of a membrane bilayer. It is connected to the vesicle through a funnel-shaped neck. The tether is of length L_t and radius R_t . It is pulled out of the vesicle by displacing a latex particle having a “point” contact with the membrane. Retraction of the tether amounts to flowing the tether material through the connecting neck. This necessarily involves in-plane shear of the membrane. The walls of the tether cylinder consist of a bilayer, *i.e.*, two molecular layers of different radii. During retraction the mass fluxes of the inner and outer monolayers have to be equal. Because the internal one is of smaller radius, the material of the inner leaflet has to flow faster than that of the external one. This induces friction between the two leaflets (intermonolayer

coupling). To model the retraction kinetics we will account for different dissipative terms relevant to our system. In contrast to lipid membranes [19], as we will see, and due to the high intrinsic viscosity of our polymer membranes, the dissipation occurs mainly within the membrane. Therefore, by modeling the tether retraction kinetics, one can estimate the magnitude of intermonolayer coupling.

In order to quantitatively describe the behavior of the relaxing tether after the bead is released, we regard the membrane as an elastic body constituted of two monolayers that can slide relative to each other. Pulling out a tether costs energy due to “bending and stretching” of the membrane. Further, we will find out that the elastic tension generated on the vesicle by this deformation, is very small—it falls within the entropic regime. Therefore, we account for an “effective” (or “entropic”) tension of the membrane [39]. Finally, the elastic energy of the bilayer after the tether is formed can be expressed as a sum of bending elasticity, stretching elasticity, non-local bending (due to differential stretching of the two monolayers) [15, 21, 40] and entropic stretching [39]:

$$W_{\text{el}} = \pi k_C L_t R_t \left(\frac{1}{R_t} - C_0 \right)^2 + \frac{1}{2} K_a \frac{(A - A_0)^2}{A_0} + \frac{1}{2} k_r \frac{(\delta A^{\text{m}} - \delta A_0^{\text{m}})^2}{A h^2} + \int_0^{A_t} \tau(A'_t) dA'_t. \quad (7)$$

Here C_0 is the spontaneous curvature of the membrane [41], k_r is the non-local bending modulus [15, 40, 42], h is the membrane thickness, δA^{m} is the area difference between the two membrane monolayers with δA_0^{m} corresponding to the relaxed equilibrium difference. For the non-local bending term we assume that the area change takes place only in the parts of the monolayers, which form the tether: $\delta A^{\text{m}} - \delta A_0^{\text{m}} \cong 2\pi L_t h$. The change in the total vesicle area can be taken roughly equal to the surface of the formed tether: $A - A_0 \cong A_t = 2\pi R_t L_t$. $\tau(A_t)$ is the entropic vesicle tension when a tether of area A_t is pulled out [39]:

$$\tau(A_t) = \tau_0 \exp\left(A_t/\tilde{A}\right), \quad \tilde{A} = A \frac{k_B T}{8\pi k_C}; \quad (8)$$

τ_0 is the surface tension of the membrane before pulling the tether. For the spontaneous curvature, we take $C_0 \cong 1/R_v$ which, compared to $1/R_t$, gives a negligible contribution.

To pull out a tether of length L_t^0 we exert a force F_{RP} on the bead held by the optical trap. The equilibrium in the static regime, before releasing the tether to retract back, is described by the minimum of the partial derivative of the free energy (7) including a term $-F_{\text{RP}} L_t$, with respect to L_t . This gives

$$\frac{\pi k_C}{R_t^0} + \frac{K_a R_t^0 A_t^0}{2R_v^2} + \frac{3k_C R_t^0 A_t^0}{2R_v^2 h^2} + 2\pi\tau_0 R_t^0 \exp\left(A_t^0/\tilde{A}\right) - F_{\text{RP}} = 0, \quad (9)$$

where $A_t^0 = 2\pi R_t^0 L_t^0$ is the initial tether area. From minimizing the elastic energy stored in the system with respect to R_t one obtains

$$-\frac{\pi k_C}{(R_t^0)^2} + \frac{K_a A_t^0}{2R_v^2} + \frac{3k_C A_t^0}{2R_v^2 h^2} + 2\pi\tau_0 \exp\left(A_t^0/\tilde{A}\right) = 0. \quad (10)$$

In the system of equations (9) and (10) we have two unknowns — the initial radius of the formed tether, R_t^0 , and the surface tension of the unperturbed vesicle, τ_0 . While the tether is well visible under phase contrast observation, the radius, R_t^0 , is not experimentally accessible and has to be determined by solving this system for R_t^0 :

$$R_t^0 = \frac{2\pi k_C}{F_{RP}}. \quad (11)$$

Typically, we find $R_t^0 \approx 0.03\text{--}0.05 \mu\text{m}$. Before we continue with assessing τ_0 , we compare the two bending terms in the elastic energy, equation (7). The non-local bending modulus k_r for lipids is reported to be about three to four times the value of the local bending modulus k_C [40, 23]. Having measured for the elastic constant K_a and k_C values close to those reported for lipids, we assume that the k_r/k_C ratio remains the same for the polymer membranes. We take $k_r = 3k_C$. Then, the non-local stretching contribution is more than two orders of magnitude smaller than the membrane bending elasticity and will be ignored in the following. In addition, we find out that the change in the relative vesicle area, $(A - A_0)/A_0$ due to the formed tether is small (less than about 5×10^{-4}). The membrane is far from the regime of elastic stretching (see Fig. 3: the elastic stretching regime starts at $(A - A_0)/A_0 \approx 5 \times 10^{-3}$). When pulling the tether we remain in the regime of “entropic” tensions [39] and further, for simplicity, we will neglect the elastic stretching term in the energy. Then for τ_0 , from equation (9) we arrive at

$$\tau_0 = \frac{k_C}{2(R_t^0)^2 \exp\left(A_t^0/\tilde{A}\right)}. \quad (12)$$

For all of our measurements we find $\tau_0 \leq 0.1 \text{ dyn/cm}$. At fully extended tethers the contribution from entropic stretching to the elastic energy is of the order of the bending term.

We will consider now the relevant dissipative contributions involved in the tether retraction. The dissipated power caused by the Stokes resistance on the sphere is $\Phi_{St} = 6\pi\eta R_b \left(\frac{dL_t}{dt}\right)^2$, where dL_t/dt is the speed of the retracting bead. The friction caused by the motion of the whole tether body modeled as a cylinder moving longitudinally is $\Phi_{Cyl} = \frac{4\pi\eta L_t}{2\ln(L_t/R_t)-1} \left(\frac{dL_t}{dt}\right)^2$ [43]. We account also for the slip occurring between the two monolayers composing the membrane [15, 16]. In lipid systems, forces induced by membrane shear flows are often neglected, as dissipation in lipid membranes is assumed to occur in the surrounding fluid [15]. However, Hochmuth *et al.* [20] estimated that in lipid membranes, shear surface viscosity contributes to about 20% to the intermonolayer friction. In

our case, the measured surface viscosity is orders of magnitude higher than the one measured in lipid membranes. Therefore, to account for possible effects of shearing the membrane, we introduce an effective shear surface viscosity, η_{eff} , in the same manner as in [20]. Essentially, η_{eff} is a superposition of the intermonolayer friction [19, 20] and the membrane shear surface viscosity

$$\eta_{\text{eff}} = bh^2 \ln(R_v/R_t) + 2\eta_s, \quad (13)$$

where b is the coefficient of interlayer slip. The contribution of the corresponding in-plane shear through the tether neck caused by the longitudinal retraction of the tether is $\Phi_{s,L} = 2\pi\eta_{\text{eff}} \left(\frac{dL_t}{dt}\right)^2$ [19, 20]. In a similar manner we account for the shear potentially caused by simultaneous shrinking (normal relaxation) of the tether radius: $\Phi_{s,R} = 2\pi\eta_{\text{eff}} \frac{L_t^2}{R_t^2} \left(\frac{dR_t}{dt}\right)^2$. The hydrodynamic dissipation in the enclosed water can be estimated as follows: in direction lateral to the tether axis we have $\Phi_{w,L} \cong \eta R_v \left(\frac{dL_t}{dt}\right)^2$, and in normal direction $\Phi_{w,R} \cong \eta L_t \left(\frac{dR_t}{dt}\right)^2$ with prefactors of order 1. To compare the different dissipative terms, we introduce the experimentally measured values for the elastic constants: $k_C \approx 1.7 \times 10^{-12} \text{ erg}^4$. For the membrane shear surface viscosity we take the value measured from the falling-ball viscosimetry experiments, $\eta_s \approx 1.5 \times 10^{-3} \text{ sp}$ (η_s enters the calculation through the effective viscosity η_{eff} , see Eq. (13); the value of b is unknown and for a lower limit one can take $\eta_{\text{eff}} = 2\eta_s$). A comparison of the different dissipative contributions shows that the only essential term for our experimental conditions is the shear dissipation, $\Phi_{s,L} + \Phi_{s,R}$. In contrast to lipid membranes [19, 20], where the leading term is the Stokes resistance, the shear dissipation in polymersome tethers surpasses the rest of the terms by about two orders of magnitude. Thus the analysis performed in [20] does not apply to our system. The tether dynamics can be described approximately by the following relationship:

$$-\frac{dW_{\text{el}}}{dt} = \Phi_{s,L} + \Phi_{s,R}. \quad (14)$$

When the system is observed from above, the tether retracts in the horizontal plane of observation⁵. While the retraction of the tether L_t is the main observable, the radius R_t is not experimentally accessible. For the analysis one can therefore consider two extreme cases: i) *Equilibrated R_t* : If the tether radius equilibration (normal relaxation) is much faster than the characteristic time of the tether retraction (longitudinal relaxation), then R_t is controlled by the minimum of the elastic energy stored in

⁴ The tether-pulling experiments were performed at 25 °C. We assume that the values of K_a and K_C , measured at 10 °C, do not vary significantly with temperature as DSC temperature scans suggest.

⁵ We suppose gravity has a negligible effect on the bead trajectory, because we did not notice any defocusing of the retracting particle. The displacement was relatively fast and the particle remained in the plane of observation. Moreover, effects due to possible flip-flop are ignored.

the system after the bead is released from the optical trap ($t \geq t_0$, $F_{RP} = 0$):

$$-\frac{\pi k_C}{(R_t)^2} + 2\pi\tau_0 \exp\left(A_t/\tilde{A}\right) = 0; \quad (15)$$

A_t/\tilde{A} is small (on the average $0.1 < A_t/\tilde{A} < 0.3$). For a rough estimate of R_t we equate the exponent in the entropic term with 1. Then,

$$R_t \approx \sqrt{\frac{k_C}{2\tau_0}}, \quad (16)$$

i.e., the tether radius stays approximately constant throughout the retraction process. For the initial moment t_0 (when $L_t = L_t^0$), the thus calculated value of the tether radius ($R_t \equiv R_t^0$) corresponds (within $\pm 5\%$) to the value of the tether radius determined from minimizing the elastic energy of the system at the moment before releasing the tether; see equation (11). ii) *Equilibrated L_t (constant R_t)*: When the longitudinal relaxation process is much faster, *i.e.*, L_t retracts very rapidly compared to the tether radius equilibration, one may assume that R_t remains roughly equal to its initial value ($R_t \cong R_t^0$). Since both approaches, i) and ii), suggest that the tether radius stays approximately constant, we do not expect these two extreme cases to give significantly different results. Hence, a more detailed analysis of the dynamics of the radius is not necessary at this stage.

We now analyze the data separately using either assumption. First, we consider the case when the tether retraction allows for equilibration of R_t . Introducing the expression for the free energy in equation (7) (we omit the elastic stretching and the non-local bending terms) into equation (14) turns the latter into an equation of motion for the tether length. The solution for L_t is

$$L_t = L_t^0 \left(1 - \frac{t - t_0}{t_R}\right), \quad (17)$$

where

$$t_R = \frac{L_t^0 \eta_{\text{eff}}}{\sqrt{2k_C \tau_0}}. \quad (18)$$

In the alternative case, where R_t is assumed to remain equal to its initial value during the tether retraction, one obtains the following time dependence:

$$g(L_t) = \frac{t - t_0}{t_L}, \quad (19)$$

where

$$g(L_t) = 1 - \frac{L_t}{L_t^0} + \frac{\tilde{A}}{A_t^0} \ln \left(\frac{1}{2} + \frac{1}{2} \exp \frac{A_t^0 - A_t}{\tilde{A}} \right) \quad (20)$$

and

$$t_L = \frac{A_t^0 \eta_{\text{eff}}}{\pi k_C} \quad (21)$$

is the characteristic relaxation time of the process.

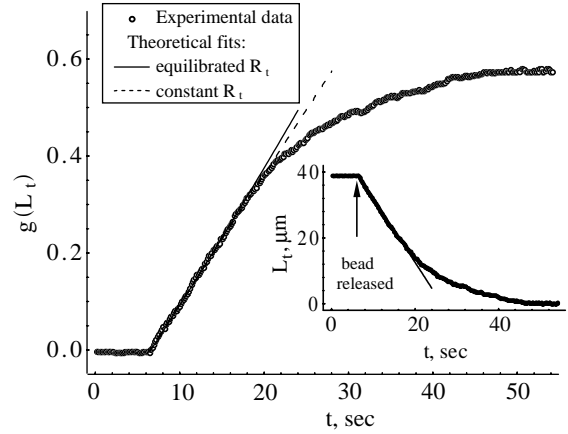


Fig. 5. Relaxation of a pulled tether in $g(L_t)$ vs. time coordinates; $g(L_t)$ is defined in equation (20). The inset presents the raw time dependence of the retracting tether length $L_t(t)$. The moment when the bead is released ($t_0 = 6.4$ s) is indicated with an arrow. The geometrical parameters of the system are: $R_v = 40 \mu\text{m}$, $R_b = 5.1 \mu\text{m}$, $R_t^0 = 0.026 \mu\text{m}$, $L_t^0 = 39 \mu\text{m}$. The solid line is a fit according to equation (17) with a single fitting parameter, $t_R = 23$ s. The dashed line is a fit following equation (19); $t_L = 39$ s.

Fitting the experimental time dependence of L_t with equation (17), provides the value of t_R , while a linear fit for $g(L_t)$ vs. time according equation (19) provides the value of t_L . These are single-parameter fits since the only unknown parameter is η_{eff} . Using equations (18) and (21), one obtains the effective viscosity η_{eff} . From equation (13) one can then estimate the intermonolayer friction coefficient b . For the characteristic thickness of the hydrophobic bilayer we have taken $h = 8 \pm 0.5$ nm. The hydrophilic PEO layer is of thickness 3 nm. These values were obtained from fitting scattering data from small-angle X-ray scattering [44]. The thickness of the polymersome membrane is approximately twice the thickness of lipid membranes.

Figure 5 gives an example for the time dependence of the function $g(L_t)$ for one vesicle calculated from the experimental data; the raw data for $L_t(t)$ is presented in the inset of the figure. The geometrical parameters of the system are indicated in the figure caption. The open circles present the set of experimental data points (the accuracy of the measurement is roughly reflected by the size of the circles). We analyzed our data using equations (17) and (19). The theoretical predictions are displayed in $g(L_t)$ vs. time coordinates; the linear fit for $L_t(t)$ according to equation (17) is displayed in the inset as well (solid line). The fits were performed for a limited L_t -interval —only down to about one particle diameter, ca $10 \mu\text{m}$. For shorter tether lengths (or distances to the vesicle body), one naturally expects slowing-down effects due to the presence of the vesicle surface. The dependence predicted by the model for equilibrated L_t (constant R_t) fits the experimental data in a larger time interval.

The results from six tether-pulling experiments on four different vesicles are presented in Table 1; see the caption for details. For the average value of the interfacial coupling

Table 1. Experimental data for six tether-pulling events. The first three experiments were performed on the same vesicle. The initial tether radius is calculated according to equation (11). The shear surface viscosity was measured on each vesicle by means of falling-ball experiments performed with a second latex particle; the viscosity of vesicle (d) was measured only with the optical dynamometry procedure. Columns (9) and (12) contain the values of the interfacial coupling constant, b , calculated correspondingly from the two relaxation times, t_R and t_L ; in brackets we give the percentage contribution of the interfacial slip, $bh^2 \ln(R_v/R_t)$, to the effective surface viscosity η_{eff} ; see equation (13). The latex particles used in all tether experiments were of radius $5 \pm 0.2 \mu\text{m}$.

(1)	(2)	(3)	(4)	(5)	(6)	(7)	(8)	(9)	(10)	(11)	(12)
Tether number (vesicle)	Vesicle radius, R_v [μm]	Initial tether length, L_i^0 [μm]	Initial tether radius, R_i^0 [μm]	Initial vesicle surface energy τ_0 , [erg/cm ²]	Shear surface viscosity, $\eta_s \cdot 10^3$ [dyn.s/cm]	Normal relaxation time t_R , [s]	Effective shear surface viscosity η_{eff} (calculated from t_R) $\times 10^3$ [dyn.s/cm]	Interfacial coupling, $b \times 10^{-8}$ [dyn.s/cm ³] (contribution to η_{eff} , %)	Longitudinal relaxation time t_L , [s]	Effective shear surface viscosity η_{eff} (calculated from t_L) $\times 10^3$ [dyn.s/cm]	Interfacial coupling, $b \times 10^{-8}$ [dyn.s/cm ³] (contribution to η_{eff} , %)
1 (a)	40	39	0.026	0.092	1.4	23	3.32	1.11 (15.7 %)	39	3.33	1.12 (15.9 %)
2 (a)	40	34	0.026	0.096	1.4	20	3.39	1.26 (17.4 %)	38	3.72	1.96 (24.7 %)
3 (a)	40	42	0.025	0.098	1.4	24	3.33	1.12 (15.9 %)	39	3.21	0.9 (12.8 %)
4 (b)	79	28	0.045	0.038	1.5	31	4.01	2.11 (25.2 %)	53	3.64	1.34 (17.6 %)
5 (c)	121	53	0.047	0.036	1.38	52	3.46	1.39 (20.2 %)	90	3.13	0.74 (11.8 %)
6 (d)	64	44	0.033	0.066	1.7	42	4.56	2.39 (25.4 %)	68	4.05	1.34 (16.0 %)

constant we obtain $b \cong (1.3 \pm 0.6) \times 10^8$ dyn s/cm³. The intermonolayer slip contributes about 20% to the effective dissipation within the membrane.

4 Discussion and conclusions

The performed experiments were aimed at estimating the mechanical and rheological properties of a novel class of polymer membranes. Interestingly, the polymersomes exhibit static elastic properties, which are not very far from those of fluid lipid membranes [4]. The bending elasticity modulus measured by micropipette aspiration is similar to that reported for lipids. For the stretching elasticity modulus we obtain values that are only slightly higher than those reported for lipids. Compared to earlier experiments on similar polymers in terms of molecular side groups and chain length [4,10], our value for the bending modulus appears to be consistent, whereas for the stretching modulus our measurement gives a significantly higher result. Clearly, systematic studies of elastic moduli as a function of chain length and hydrophilic to hydrophobic fraction are needed.

Our major new insight concerns the viscous characteristics of these membranes. We measured the shear surface viscosity and made an estimation of the interlayer viscous drag. If we compare the present viscosity measurements on polymersomes with the same measurements on lipid SOPC or DMPC vesicles [8,9], we find the striking fact that the viscosity of polymer membranes is about 500 times larger. The slow dynamics in the polymer membranes is obvious already when following the mobility of the latex probe: while for a lipid vesicle of radius 40 μm a bead of radius 5 μm takes about 2 min to span the pole-to-pole vesicle distance, for the polymersomes this time is more than 2 hours.

The tether-pulling experiments we performed provide a supplementary insight into the properties of polymer membranes. We analyzed our experiments testing two models for the relaxation process of the tether that give very similar results. Comparison of the friction terms shows that effective surface viscosity (η_{eff}) is the main source of dissipation of which intermonolayer friction constitutes about 20%. The interfacial coupling constant b turns out to be an order of magnitude higher than those of lipid membranes, where the reported values for b are between 10^6 and 10^7 dyn s/cm³ [15,28]. A plausible explanation for the high interfacial drag is the structure of the polymer molecule. Having a “single-tail” hydrophobic part, in comparison with the two tails of the lipid molecules, it might be easier for a polymer molecule from one monolayer to interpenetrate in the opposing monolayer and thus render the monolayer slip difficult.

In addition, a closer look at our analysis of the tether-pulling experiments suggests that one can introduce an arbitrary energy contribution, which can be linearized around the tether area. Inserted in the energy expression, equation (7), such a linear term will lead to the same types of solutions for the dynamics of the retracting tether. Interestingly, this contribution could also be an adhesion energy term eventually induced by the contact of our vesicles with the electrode or adjacent vesicles. In this sense our analyses appear to be quite robust.

Because of the relatively low value of the measured bending elasticity modulus for the polymer membranes, one would expect to see thermal shape fluctuations for deflated (with excess area) vesicles. However, these membrane undulations are extremely slow. Detailed analysis of the membrane fluctuation behavior and its temperature dependence will be the object of future work. For normal lipids, membrane undulations are damped out by the surrounding media (*e.g.*, water) viscosity [45]. In contrast, the intuitive conjecture for the polymer membranes

is that the large characteristic times of the undulations are mainly due to viscous dissipation within the bilayer membrane.

Compared to lipids, synthetic polymer chains can offer an ample diversity in designing novel artificial membranes with specific mechanical characteristics. The preparation and characterization of special membranes of enhanced robustness and stiffness from purely artificial or biologically modified compounds is rather inviting with regard to fields like rheology and transport, encapsulation, drug and gene delivery. The possibility to include polymeric segments that respond to pH, ionic strength or temperature would further allow to specifically control membrane functions in different biological environments. In addition, a special property of some polymer membranes, depending on the particular chemistry of the molecules, is the possibility for a lateral crosslinking within the membrane, which can turn vesicles into solid-like shells (see, *e.g.*, [46]). Polymerized vesicles are potentially suitable for areas like oral drug delivery [47].

References

1. F.S. Bates, G.H. Fredrickson, *Physics Today*, February issue, Vol. **32** (1999).
2. K. Yu, A. Eisenberg, *Macromolecules* **31**, 3509 (1998).
3. N.S. Cameron, M.K. Corbierre, A. Eisenberg, *Can. J. Chem.* **77**, 1311 (1999).
4. B. Discher, Y.-Y. Won, D. Ege, J. Lee, F. Bates, D. Discher, D. Hammer, *Science* **284**, 1143 (1999).
5. D. Marsh, *CRC Handbook of Lipid Bilayers* (CRC Press, Boca Raton, Ann Arbor, Boston, 1990).
6. L. Fisher, A. Blume (Editors), *Characterization of Bilayers*, in *Curr. Opin. Colloid Interface Sci.*, Vol. **5** (2000).
7. U. Seifert, *Adv. Physics* **46**, 13 (1997).
8. R. Dimova, C. Dietrich, A. Hadjiisky, K. Danov, B. Pouligny, *Eur. Phys. J. B* **12**, 589 (1999).
9. R. Dimova, B. Pouligny, C. Dietrich, *Biophys. J.* **79**, 340 (2000).
10. J.C.-M. Lee, H. Bermudez, B.M. Discher, M.A. Sheehan, Y.-Y. Won, F.S. Bates, D. Discher, *Biotechnol. Bioeng.* **73**, 135 (2001).
11. J.K. Mills, D. Needham, *Expert Opin. Therap. Patents* **9**, 1499 (1999).
12. B. Discher, D. Hammer, F. Bates, D. Discher, *Curr. Opin. Colloid Interface Sci.* **5**, 125 (2000).
13. S. Förster, E. Krämer, *Macromolecules* **32**, 2783 (1999).
14. H.-G. Döbereiner, *Curr. Opin. Colloid Interface Sci.* **5**, 256 (2000).
15. E. Evans, A. Yeung, R. Waugh, J. Song, in *The Structure and Conformation of Amphiphilic Membranes*, edited by R. Lipowsky, D. Richter, K. Kremer, *Springer Proc. Phys.*, Vol. **66** (Springer, Berlin Heidelberg New York, 1992) p. 148.
16. U. Seifert, S.A. Langer, *Europhys. Lett.* **23**, 71 (1993).
17. A. Yeung, E. Evans, *J. Phys. II* **5**, 1501 (1995).
18. K. Velikov, C. Dietrich, A. Hadjiisky, K. Danov, B. Pouligny, *Europhys. Lett.* **40**, 405 (1997).
19. E. Evans, A. Yeung, *Chem. Phys. Lipids* **73**, 39 (1994).
20. R. Hochmuth, J.-Y. Shao, J. Dai, M. Sheetz, *Biophys. J.* **70**, 358 (1996).
21. S. Svetina, B. Zeks, R.E. Waugh, R.M. Raphael, *Eur. Biophys. J.* **27**, 197 (1998).
22. R.E. Waugh, *Biophys. J.* **38**, 19, 29 (1982).
23. R. Raphael, R. Waugh, *Biophys. J.* **71**, 1374 (1996).
24. L. Bo, R.E. Waugh, *Biophys. J.* **55**, 509 (1989).
25. V. Heinrich, R.E. Waugh, *Ann. Biomed. Eng.* **24**, 595 (1996).
26. V. Heinrich, B. Bozic, S. Svetina, B. Zeks, *Biophys. J.* **76**, 2056 (1999).
27. H.-G. Döbereiner, *Biophys. J.* **76**, 1723 (1999).
28. R. Merkel, E. Sackmann, E. Evans, *J. Phys. (Paris)* **50**, 1535 (1989).
29. E. Evans, W. Rawicz, *Phys. Rev. Lett.* **64**, 2094 (1990).
30. E. Evans, D. Needham, *J. Phys. Chem.* **91**, 4219 (1987).
31. L. Xu, H.-G. Döbereiner, in *Giant Vesicles*, edited by P. Luisi, P. Walde (Wiley & Sons, 2000) p. 181.
32. See, *e.g.*, M. Angelova, in *Giant Vesicles*, edited by P. Luisi, P. Walde (Wiley & Sons, 2000) p. 29.
33. P. Méléard, C. Gerbaud, T. Pott, M.D. Mitov, in *Giant Vesicles*, edited by P. Luisi, P. Walde (Wiley & Sons, 2000) p. 185.
34. W. Rawicz, K.C. Olbrich, T. McIntosh, D. Needham, E. Evans, *Biophys. J.* **79**, 328 (2000).
35. M. Angelova, B. Pouligny, *Pure Appl. Opt. A* **2**, 261 (1993).
36. C. Dietrich, M.I. Angelova, B. Pouligny, *J. Phys. II* **7**, 1651 (1997).
37. W. Helfrich, R.-M. Servuss, *Nuovo Cimento D* **3**, 137 (1984).
38. K. Danov, R. Dimova, B. Pouligny, *Phys. Fluids* **12**, 2711 (2000).
39. U. Seifert, *Z. Phys. B* **97**, 299 (1995).
40. R. Waugh, J. Song, S. Svetina, B. Zeks, *Biophys. J.* **61**, 974 (1992).
41. W. Helfrich, *Z. Naturforsch.* **28c**, 693 (1973).
42. L. Miao, U. Seifert, M. Wortis, H.-G. Döbereiner, *Phys. Rev. E* **49**, 5389 (1994).
43. C. Pozrikidis, *Introduction to Theoretical and Computational Fluid Dynamics* (Oxford University Press, New York, 1997).
44. S. Förster, H. Schnablegger, U. Borchert, S.E. Funari, S. Cunis, P. Lindner, in preparation.
45. S.T. Milner, S.A. Safran, *Phys. Rev. A* **36**, 4371 (1987).
46. T. Komatsu, E. Tsuchida, C. Boettcher, D. Donner, C. Messerschmidt, U. Siggel, W. Stocker, J. Rabe, J.-H. Fuhrhop, *J. Am. Chem. Soc.* **119**, 11660 (1997).
47. J. Okada, S. Cohen, R. Langer, *Pharmaceut. Res.* **12**, 576 (1995).